NANO LETTERS

Letter

pubs.acs.org/NanoLett

Nanowire Substrate-Based Laser Scanning Cytometry for Quantitation of Circulating Tumor Cells

Sang-Kwon Lee,*[,†,‡] Gil-Sung Kim,[‡] Yu Wu,[†] Dong-Joo Kim,[‡] Yao Lu,[†] Minsuk Kwak,[†] Lin Han,[†] Jung-Hwan Hyung,[‡] Jin-Kyeong Seol,[‡] Chantal Sander,[†] Anjelica Gonzalez,[†] Jie Li,[§] and Rong Fan*[,†,∥]

[†]Department of Biomedical Engineering, Yale University, New Haven, Connecticut 06511, United States

[‡]Department of Semiconductor Science and Technology, Chonbuk National University, Jeonju 561-756, Korea

[§]Department of Neuropathology, Yale School of Medicine, New Haven, Connecticut 06520, United States

[∥]Yale Comprehensive Cancer Center, New Haven, Connecticut 06520, United States

S *Supporting Information*

ABSTRACT: We report on the development of a nanowire substrate-enabled laser scanning imaging cytometry for rare cell analysis in order to achieve quantitative, automated, and functional evaluation of circulating tumor cells. Immunofunctionalized nanowire arrays have been demonstrated as a superior material to capture rare cells from heterogeneous cell populations. The laser scanning cytometry method enables large-area, automated quantitation of captured cells and rapid evaluation of functional cellular parameters (e.g., size, shape, and signaling protein) at the single-cell level. This integrated platform was first tested for capture and quantitation of human lung carcinoma cells from a mixture of tumor cells and leukocytes. We further applied it to the analysis of rare tumor cells spiked in fresh human whole blood (several cells per mL) that emulate metastatic cancer patient blood and demonstrated the potential of this technology for analyzing circulating tumor cells in the clinical settings. Using a high-content image analysis algorithm, cellular morphometric parameters and fluorescence intensities can be rapidly quantitated in an automated, unbiased, and standardized manner. Together, this approach enables informative characterization of captured cells in situ and potentially allows for subclassification of circulating tumor cells, a key step toward the identification of true metastasis-initiating cells. Thus, this nanoenabled platform holds great potential for studying the biology of rare tumor cells and for differential diagnosis of cancer progression and metastasis.

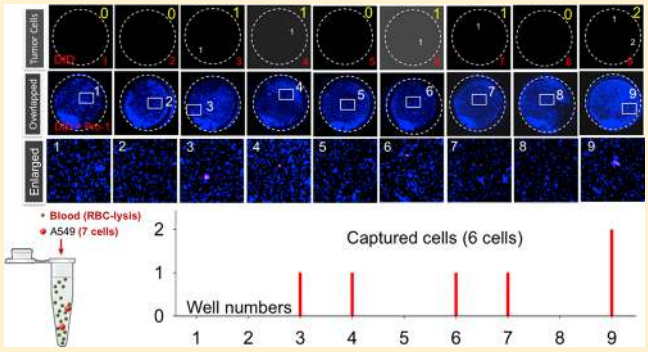

KEYWORDS: *Circulating tumor cells, quartz nanowire array, laser scanning cytometry, cellomic analysis*

In recent years, there has been a great surge of interest in utilizing the peripheral blood circulating tumor cells (CTCs) to predict the likelihood of cancer metastasis and monitor the therapeutic responses of patients.[1,2] CTCs are shed by both primary and metastatic tumors, and they are thought to mediate the hematogenous spread of cancer to distant sites.[3,4] Despite the clinical and pathophysiological importance of CTCs, the utility of these cells as a cancer biomarker is limited by the availability of reliable technologies for efficient capture and functional characterization of CTCs. The difficulty resides in many aspects, including the rarity and heterogeneity of CTCs in blood. It was estimated that CTCs are present at extremely low abundance (1−100 CTCs/mL) in a noisy background of highly abundant hematologic cells (~10^9 cells/mL) in the whole blood. To date, several technologies, such as magnetic separation using immunofunctionalized magnetic beads, cell size-based mechanical separation, and microstructure-facilitated cell capture, have been developed in hope to isolate, detect, and count CTCs.[5−14] Recent reports on cell−nanostructure interaction have shown that nanometer scale topography influences not only diverse cell behavior, such as cell adhesion, motility, proliferation, and differentiation,[7,8,15−26] but also the performance (efficiency and yield) of nanostructure-based cell capture.[27−31] For example, a silicon nanowire (SiNW) substrate coated with an antibody against epithelial cell adhesion molecules (e.g., EpCAM) exhibited high capture efficiency when employed to isolate EpCAM-positive CTCs.[28,29] All these technological advances point to the possibility of using nanostructured substrates to capture very rare cell populations including CTCs. To meet the stringent criteria of clinical CTC analysis, it is required to develop rapid quantitation of CTCs in an automated manner. Moreover, owing to the low numbers of CTCs one can separate from clinical specimens and the inherent heterogeneity of these cells, it is of vital importance to

Received: November 28, 2011
Revised: May 29, 2012
Published: May 30, 2012

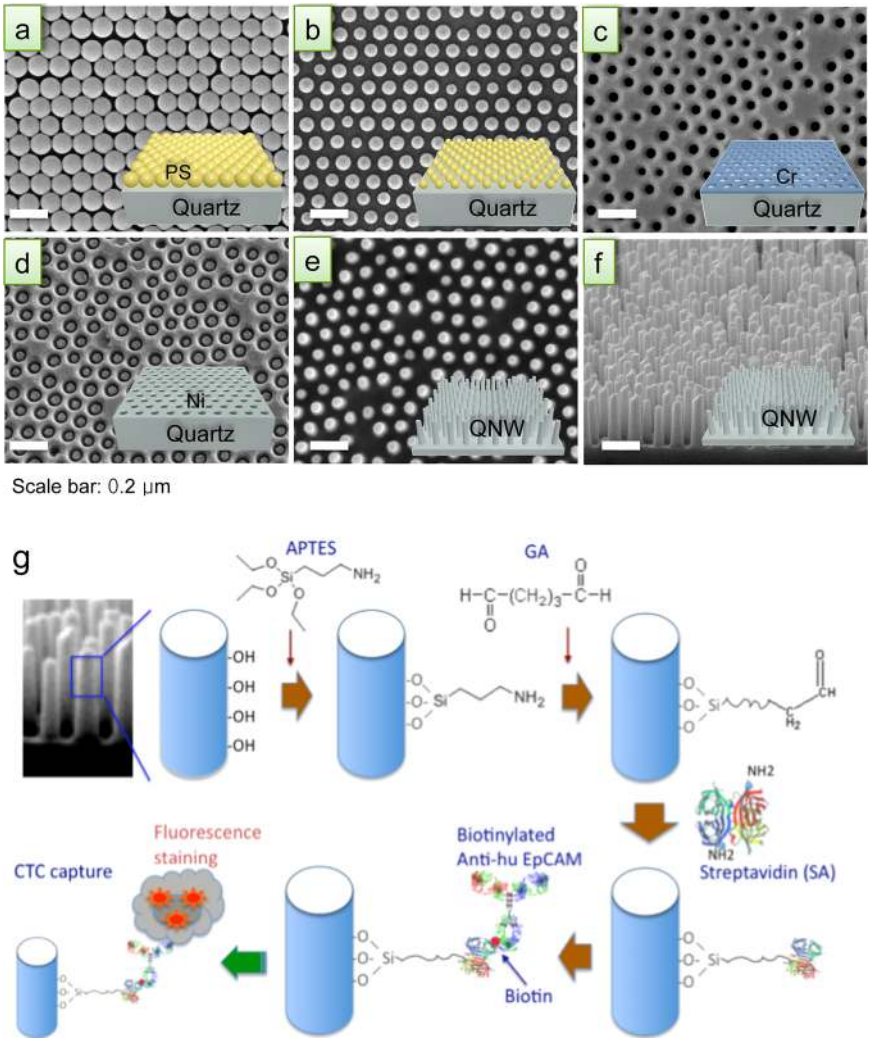

Figure 1. Fabrication and surface functionalization of QNW arrays. (a) Spin-coating process of PS NPs on a flat quartz substrate. The size of the PS NPs was ~100 nm. (b) First O_2 plasma etching for size reduction of coated PS NPs. (c) Cr metal deposition (25 nm) using e-beam evaporator and lift-off of PS NPs with *N*-methy1-2-pyrrolidone (NMP). (d) Ni metal deposition used as an etch mask and Cr metal lift-off process. (e,f) Second plasma etching (top- and tilted-view, respectively). RIE was performed to fabricate the QNW arrays with SF_4/Ar gas for 4 min. After RIE, the remaining Ni metal was completely removed with a wet-etchant (LCE-12K, Cyantek, USA). (g) Depiction of the step-by-step functionalization of nanowire surface with APTES, GA, streptavidin, and biotinylated antihuman EpCAM antibody for circulating tumor cell capture.

comprehensively characterize the functions of captured CTCs in situ in order to distinguish CTC subtypes or even metastasis-initiating cells. This is such a paramount endeavor to promote the current CTC analysis technologies to the stage of clinical utilization of CTCs as fluid biopsies for cytopathological examination and differential diagnosis of cancer metastasis.

Laser scanning cytometry (LSC) emerges as a powerful technology for high-content, high-throughput quantitative analysis of cellular functions in a fully automated manner.[32,33] It utilizes large-area fluorescence imaging schemes and rigorous image quantitation algorithms to enable informative analysis of cell samples attached to a solid substrate, making it more amenable to the study of heterogeneous cell populations. Using either morphometric or proteomic analysis, one can generate a suite of quantitative metrics to comprehensively characterize all single cells immobilized on the substrate. While this technology represents a powerful approach for high-content screening using cell lines, it has not been applied to the study of rare cells in clinical specimens, which is challenging because it lacks the capability of rare cell capture and separation.

Herein, we integrate a nanowire substrate that serves as an efficient cell capture tool and laser scanning cytometry that works for quantitative, automated characterization of captured rare cells to yield an integrated, nanoenabled platform for informative analysis of CTCs. In order to capture very rare tumor cells in clinical blood samples (several tumor cells per mL), large volumes of clinical samples (~mL) need to be examined, for example, by flowing through a microfluidic cell capture apparatus to isolate and enrich circulating tumor cells.[9] Using the nanowire substrate-based imaging cytometry, we can directly apply large volumes of blood samples onto a large-area nanowire substrate, which can be imaged by laser scanning cytometry for accurate identification of all tumor cells. We also conducted informative morphometric analysis of all tumor cells captured on the substrate using high-content image analysis algorithms. When fluorescence-labeled antibodies were used to measure cell surface markers or cytoplasmic signaling proteins, it could also yield proteomic profiles of single tumor cells in hope of identifying molecular signatures and signaling pathways for CTC subclassification. Such technology integration is not

dx.doi.org/10.1021/nl2041707 | *Nano Lett.* 2012, 12, 2697–2704

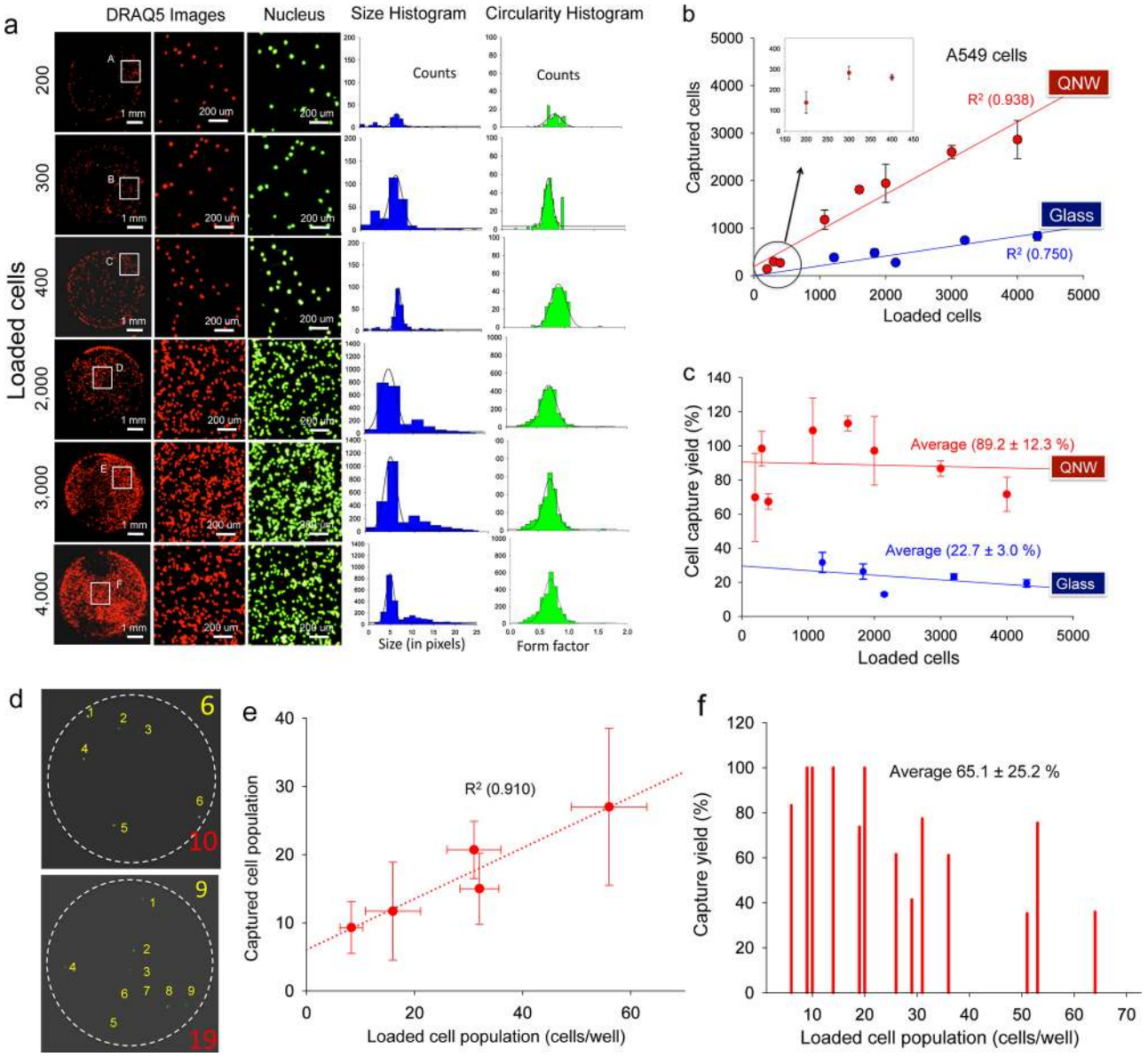

Figure 2. Imaging and quantitation of lung carcinoma cells captured on nanowire arrays. (a) First and second column: low magnification and enlarged fluorescence images (white box region shown in A–F) of captured human lung tumor cells (A549) on STR-functionalized QNW arrays bound with PDMS wells for different loaded cell populations in the range of 200–4000 cells/well. Third column: CellProfiler generated outlined images of captured cells on STR-QNW arrays for cell counting. Forth and fifth column: size and circularity histogram of immobilized A549 cells on STR-functionalized QNW arrays. The circularity (also known as form factor, ff), which is calculated as $[4\pi(\text{area})/(\text{perimeter})^2]$, represents the criterion of the circularity of the immobilized cells. If the ff = 1, then the captured object is a perfect circular object. The solid line represents a Gaussian fitting. (b) Correlation of total captured cells (A549) on STR-functionalized QNW arrays and STR-planar glass substrate versus loaded cells from cell suspension ($R^2 \sim 0.94$ and ~0.75 for STR-QNW and STR-planar glass, respectively). Each result and error bar represents an average with standard deviation from three repeats ($n = 3$). (c) Cell capture efficiency (yield) of the captured cells (A549) on two different topographies of substrates, STR-QNW arrays, and STR-planar glass substrate as a function of loaded cells in the range of 200–4300 cells/well. The solid-line represents a linear fitting. Each result and error bar represent an average with standard deviation ($n = 3$). (d) Representative fluorescence images of captured A549 cells (human lung tumor cells) on STR-QNW arrays with cell loading in the range of 10–64 cells/sample. The captured cells were prestained by green-Vybrant DiI and scanned by microarray scanner. The immobilized cell population was then counted manually and also compared to the images from optical and fluorescence microscopy. Yellow-colored numbers (right-top) denote the number of captured cells for each well, while red-colored numbers (right-bottom) indicate the total loaded cell population. (e) Correlation of total captured cells on STR-QNW arrays as a function of the loaded cells from cell suspension in the range of 6–64 cells/well, indicating a good linear relationship with the loaded cell population. The dotted line represents a linear fitting ($R^2 = 0.910$). Each result shows an average with standard deviation ($n = 3$). (f) Cell capture yield distribution versus loaded cell population in the range of 6–64 cells/well.

trivial. It aims to bridge the gap between prototype technology and clinical use in order to facilitate the translation of a promising nano-enabled rare cell analysis platform to diagnosis and the stratification of metastatic cancers.

Fabrication and Functionalization of Transparent Quartz Nanowire Arrays. The fabrication procedure for the transparent quartz nanowire (QNW) arrays is illustrated in Figure 1. It went through a series of processes including

dx.doi.org/10.1021/nl2041707 | *Nano Lett.* 2012, 12, 2697–2704

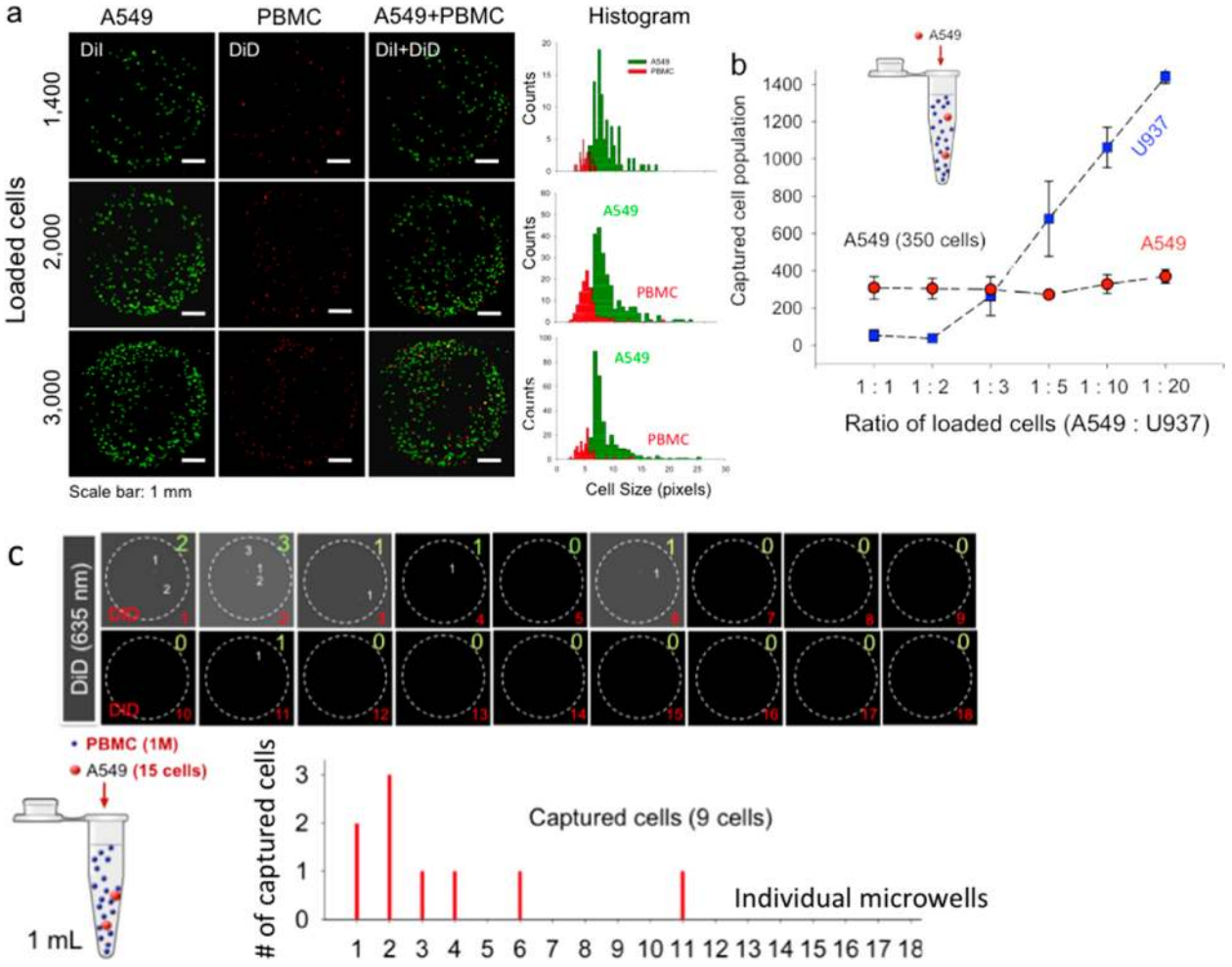

Figure 3. Capture of lung carcinoma cells from mixed cell populations. (a) Scanned images of captured cells from the mixture of A549 (green labeled) and PBMCs (red labeled) using nanowire arrays and the size distribution in pixels. A549/PBMC on STR-QNW arrays as a function of loaded cells in the range of 1400−3000 cells/well. (b) Both tumor cells (A549) and monocyte/background cells (U937) captured on nanowire substrate as a function of the ratio A549/U937 when the same amount of A549 cells were spiked in different densities of U937 cells. The result shows the tumor cell capture yield remains relatively constant although the nonspecific capture of background cells significantly varies with the PBMC cell density. (c) Capture of rare tumor cells spiked in as-received PBMCs. Scanned images of tumor cells captured from an as-received human PBMC sample spiked with A549 lung cancer cells (15 cancer cells in 1 mL PBMC suspension). Tumor cells were prestained with membrane dye DiD.

nanoparticle coating, metal deposition, pattern transfer, and deep reactive ion etching to generate vertical nanowires. Polystyrene nanoparticles (PS NPs) were applied onto a quartz wafer using either spin-casting or dip-coating. The resulting pattern exhibits short-range ordering in a close-packed manner. The size of the PS NPs can be further shrunk using oxygen plasma etching. Then these particles served as a template to deposit chromium metal forming a nanohole pattern that was inverted to yield a nanodot pattern using nickel deposition and selective chrome etching. Finally, the nanodot pattern was transferred down to the quartz substrate using oxide reactive ion etching, producing an array of QNWs. The typical diameter and length range from 80 to 100 nm and 250 to 350 nm, respectively (Figure 1f). The QNW array substrate is completely transparent and suitable for optical examination (both phase contrast and fluorescence) of captured tumor cells.

The nanowire substrate was then functionalized with monoclonal antihuman EpCAM antibody using a streptavidin-immobilization method[34] (Figure 1g). During this procedure, as-prepared QNWs were treated with oxygen plasma to render a surface with high density of silanol group. Then we applied (3-aminopropyl)-triethoxysilane (APTES) to aminate the nanowire surface, which can be further functionalized with streptavidin (STR) via a two-step aldehyde/amine reaction and using glutaraldehyde (GA) as the linker. Finally, biotinylated antihuman EpCAM was introduced to the STR-functionalized nanowires, which, through the high-affinity biotin−streptavidin binding, yielded a immunofunctionalized nanowire surface coated with antihuman EpCAM antibodies. EpCAM is a pan-epithelial cell surface marker and presumably EpCAM+ cells captured from blood are carcinoma cells shed into the bloodstream.

Automated Imaging and Quantitation of Tumor Cells Captured on Nanowire Substrates. In order to accurately count and characterize very rare tumor cells, such as CTCs, with good statistic power, large quantities of blood samples need to be analyzed per individual patient, suggesting the need of large-area nanowire substrates (>1 in. × 1 in.) to handle the large volume of sample and ensure high-yield capture of CTCs. However it is not reliable for clinicians to perform counting or

dx.doi.org/10.1021/nl2041707 | *Nano Lett.* 2012, 12, 2697−2704

characterization of captured cells over such a large area using a conventional hemocytometer method. Here we exploited a rapid laser scanning cytometry approach to automatically quantitate all single cells captured on the substrate using a simple microarray scanner. Two laser beams (635 and 532 nm) were employed to measure fluorescence-stained tumor cells (see Supporting Information).[35] This approach can be fully automated and standardized for the use in clinical laboratories.

To evaluate cell capture and imaging capability, we first conducted a set of experiments using pure tumor cell samples. Cell suspensions were prepared at densities (A549, human lung carcinoma cells) ranging from ~200 to 4300 cells per test sample (100 μL) onto a set of PDMS microwells assembled on EpCAM functionalized QNW arrays. Figure 2a shows scanned images of A549 tumor cells captured on an antihuman EpCAM-functionalized QNW substrate as well as quantitative analyses of cellular parameters. The first and second columns show original fluorescence images, and the third column shows the result of automated identification of cell shape (cell boundary shown in green) for morphometric analysis. In our experiments, we were able to simultaneously extract a dozen physical parameters, and in Figure 2a (the fourth and fifth columns), we show two parameters for all single tumor cells we captured—one is the cell size and the other is cell circularity. It was found that the average size of immobilized A549 cells was ~190.0 ± 94.8 μm^2, which is in good agreement with the estimation using epifluorescence imaging (Figure S1, Supporting Information). Cell circularity analysis indicates that most as-captured cells are round with a typical roundness factor ~0.88. The observed homogeneity of morphometric parameters in all single tumor cells are what we expected because the same cell line was used in all these experiments. However, CTCs from patients are expected to be highly heterogeneous, and the capability for multiparameter functional (including morphometric) analysis is useful for distinguishing CTC subsets and differential diagnosis.

We also performed A549 tumor cell capture using anti-EpCAM functionalized flat glass substrates, and the results are shown in Figure S2, Supporting Information. Then we conducted a quantitative comparison of tumor cell capture efficiency between these two platforms and at varying cell densities (Figure 2b,c). The result from nanowire substrates shows a nearly linear correlation between the number of captured cells vs loaded cells for up to 4000 cells (n = 3, R^2 = 0.94). The flat glass platform yields a lower regression, of approximately 0.75, than that of nanowire arrays, which indicates a higher cell−substrate interaction on nanowire arrays as compared to the flat glass substrate. This result is consistent with prior reports.[20,21] Figure 2c shows the cell capture yield, which is defined as the percentage of captured cells to all cells initially loaded. It was found that the capture yield remains relatively constant over the wide range of cell density. The nanowire substrate gives rise to a substantially higher yield than the flat glass substrates.

In order to image small numbers of tumor cells captured on nanowire arrays, we added human lung cancer cells (A549) prelabeled with Dil (Invitrogen) to a culture medium with nominal cell numbers ranging from 10 to 64 per test well (100 μL). Figure 2d shows the representative scanned images of two microwells. The number of loaded cells in each test well is shown in red at the lower right corner, while the number of captured cells is shown in yellow at the upper right corner. The average capture yield is ~65.1 ± 25.2% (Figure 2e,f). These results demonstrated that we can accurately count captured cells using the imaging cytometry approach when the cell number is very low.

Quantitation of Rare Tumor Cells from Mixed Cell Populations. Here we take one step further to assess the utility of nanowire substrate-based laser imaging cytometry for CTC analysis in the settings close to clinical diagnosis; captured from mixed cell populations that can mimic patient specimen to some extent. Lung cancer cells (A549) were spiked at varying cell densities into the suspensions of human peripheral blood mononuclear cells (PBMCs) to perform tumor cell capture experiments. We also studied the mixed cell populations by spiking A549 cells to human monocytic cells (U937) (Figures S3 and S4, Supporting Information). As shown in Figure 3a, the first and the second columns show single channel scanned images of all cells captured in a representative microwell loaded with the mixture of A549 cells and PBMCs. Tumor cells were prestained with green membrane dye Dil and all PBMCs prestained with red membrane dye DiD. The third column is the overlay of both channels. The histogram showing the quantitative image analysis of cell size distribution indicates tumor cells (~20−40 μm) are generally larger than PBMCs (~5−15 μm), manifesting the potential utility of single cell morphometric analysis for distinguishing heterogeneous cell populations. Next we systematically studied the effect of background cells on the capture yield and purity by varying the ratio of tumor and background cells. U937, a human monocytic cell line, was used as the background cells. The result indicates the capture yield of target cells (tumor cells) is relatively constant, whereas the background cells do show elevated nonspecific capture with increasing their density (Figure 3b and Figures S8 and S9, Supporting Information). Finally we demonstrated the capture of rare tumor cells spiked in PBMCs at a density equivalent to clinical cancer patient samples. In this experiment, the entire chip containing 18 PDMS microwells was used to measure one sample. Automated imaging cytometry can visualize the whole chip and rapidly identify the total number of tumor cells captured from all the microwells. Figure 3c shows the raw scanned fluorescence images of each microwell (labeled 1−18) after cell capture experiment, and the tumor cell capture yield is 9 out of 15 cells spiked in the PBMC sample, demonstrating the applicability of our technology for quantitation of rare tumor cells from heterogeneous cell samples.

Human Whole Blood Samples to Assess the Utility for Clinical CTC Analysis. We used fresh whole blood samples from two volunteers and two brain tumor patients to assess the utility of our technology for quantitative analysis of rare tumor cells by spiking ultralow abundance A549 cells in whole blood (several A549 cells per mL of blood). These spiked samples are almost identical to the blood samples from metastatic cancer patients. The experiment procedure is the following: First, these whole blood samples were spiked with A549 cells at a level of ~10 cells per mL. Second, RBC-lysis solution was added to the spiked whole blood samples and incubated for 10 min at room temperature to remove red blood cells that may complicate fluorescence imaging. Third, the remaining cells were spun down to remove debris and resuspended in the same volume of medium for cell capture experiment. Fourth, these samples containing rare tumor cells (~7 or 15 cells per mL) was introduced onto the entire nanowire substrate chip, on which there are 18 PDMS wells, and each contains ~60 μL of sample. The total volume of blood analyzed using a nanowire

dx.doi.org/10.1021/nl2041707 | Nano Lett. 2012, 12, 2697−2704

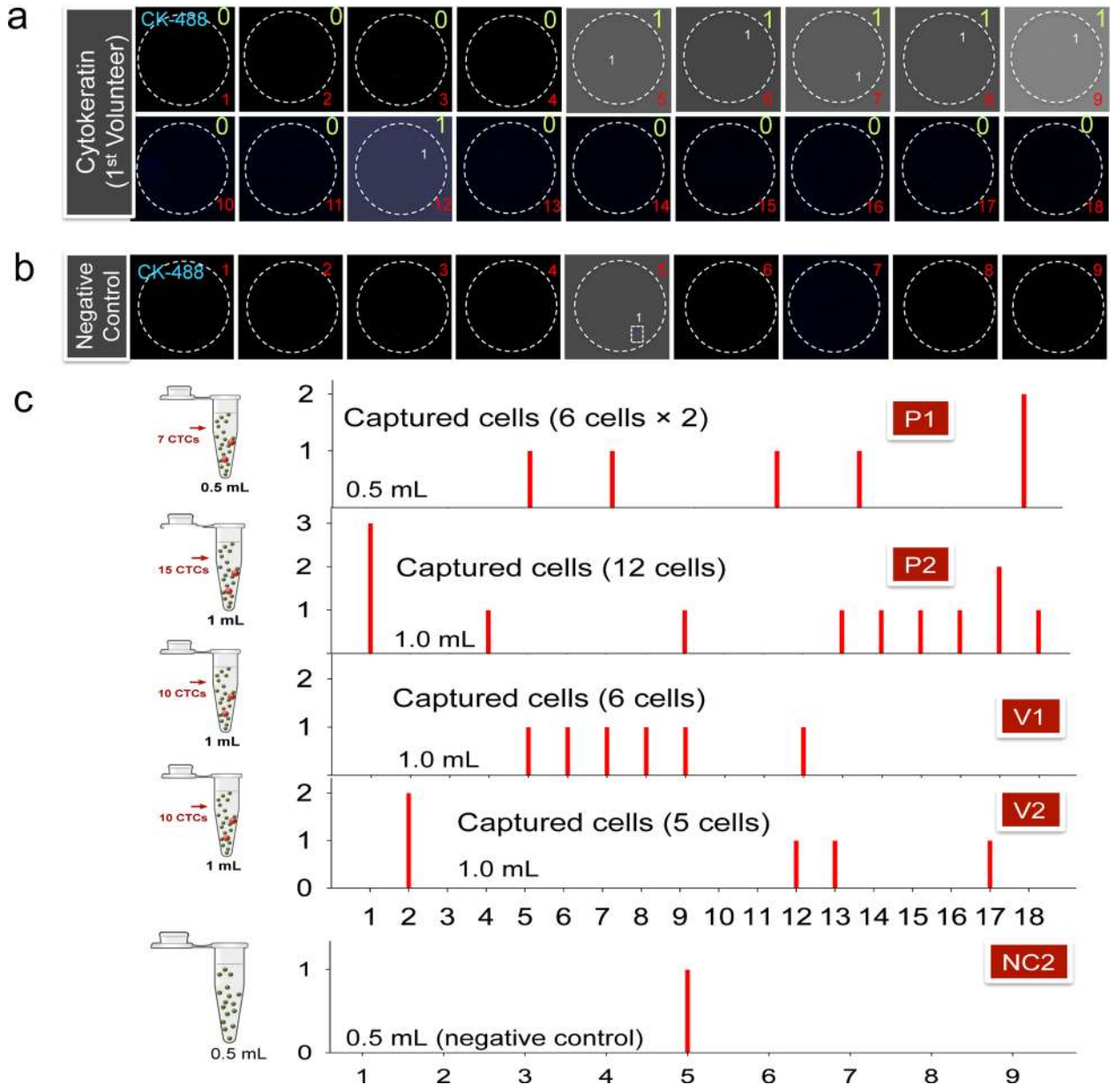

Figure 4. Capture, imaging and quantitation of lung cancer cells spiked in fresh human whole blood samples. (a) Scanned images of captured tumor cells on STR-functionalized NW substrates where only ~10 cells spiked into human whole blood sample. Typically, the whole blood sample (3 mL) was collected from either healthy volunteers (V1 and V2) or primary brain tumor patients (P1 and P2). Ten A549 cells were then spiked into 1 mL of RBC-lysed blood. The mock metastatic patient blood samples were evenly aliquoted and loaded into 18 microwells on top of a nanowire substrate. To identify captured CTCs from numerous other cellular components of lysed whole blood, the samples were stained with DRAQ-5 (red 665 nm) and fluorescence-conjugated anticytokerain (blue 488 nm, eBioscience, USA) for all nuclei and epithelial tumor cells, respectively. Green-colored numbers (right-top) for each microarray scanned image (top of the first row) denote the number of captured cells for each well, while red-colored numbers (right-bottom) indicate the microwells numbered 1−18. Using dual-color imaging, the tumor cells show purple (dual positive, red-DRAQ-5+/blue-CK-488+), while all the cells including nonspecific cells can be identified by nuclear dye (no shown). (b) Microarray scanned images of negative control sample (as-marked NC2) from the same blood samples (V2) used for preparing spiked blood samples. (c) Summary of the captured cells for two peripheral patient samples (P1 and P2) and two volunteer blood samples (V1 and V2), showing the average capture yield to be ~67.5 ± 15% (n = 4). Ten cells of A549 (CTCs) with final volume of 1 mL were used for the capture experiments.

substrate is 18 × 60 = 1080 μL or ~1 mL. Cells were incubated on the nanowire array for 30−60 min for cell capture followed by a rinsing step. For each sample, we also measured unspiked blood for negative control (Figure S7, Supporting Information). Finally, all the captured cells were fixed by 4% PFA in PBS buffer, stained with phycoerythrin (PE)-conjugated anticytokeratin and YO-PRO-1 for 30 min at room temperature. Afterward, captured cells were imaged using laser scanning cytometry to obtain cell count, cell size, shape, and fluorescence intensity of each cell over the entire substrate (Figures S5 and S6, Supporting Information).

Figure 4a shows the scanned images of all the microwells used to analyze a human blood sample (volunteer V1) using PE-conjugated anticytokeratin, whereas Figure 4b is the raw images for negative control (no tumor cells spiked). Figure 4c summarized the quantitative counts of captured tumor cells

dx.doi.org/10.1021/nl2041707 | Nano Lett. 2012, 12, 2697−2704

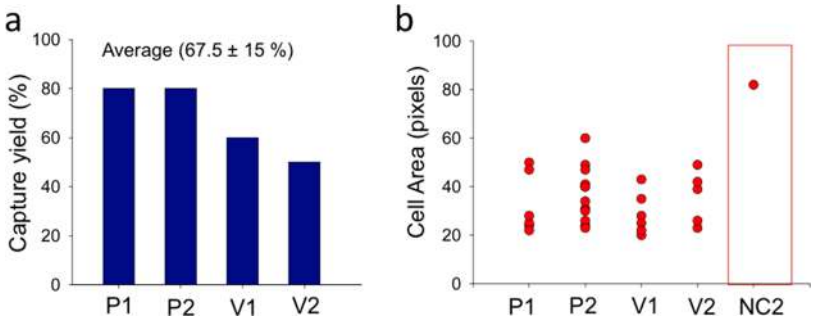

Figure 5. Quantitation and characterization of tumor cells captured from human blood samples. (a) Tumor cell capture yield (the number of captured tumor cells as visualized by fluorescent marker vs the nominal number of tumor cells spiked in 1 mL of the whole blood sample). P1, P1, V1, and V2 denote samples from brain tumor patient 1 and 2 and healthy volunteers 1 and 2. (2) Cell size quantified for all captured tumor cells from four blood samples (P1, P2, V1, and V2) and one of the negative controls (NC2).

from all four human blood samples (P1, P2, V1, and V2) as well as from a negative control sample. Then we can determine the capture yield for these whole blood samples spiked with low-abundance tumor cells (Figure 5a), and the average capture yield is ~67.5 ± 15.0%. This result indicates a greater performance as compared to previous stationary nanowire-based CTC capture presumably due to the large-area of nanowire substrate and large-scale imaging capability. The imaging cytometry approach also allows for rapid quantitation of cellular parameters, such as cell size (Figure 5b). Apparently the size distribution is similar for these samples, which is as expected because the same type of tumor cells (A549) were used in all the human blood sample experiments. Finally, we almost could not detect tumor cells from negative control samples according to the fluorescence signal. Only in one of all the negative control samples we observed a false signal (Figure 4b). However quantitation indicates the size of that "tumor cell" is much larger than others (Figure 5b), suggesting that imaging cytometry-based morphometric characterization may help remove false positive signals and more accurately quantitate tumor cells.

In summary, we report on a nano-enable technology platform for high-yield capture and rapid analysis of rare cells by integrating biofunctionalized QNW arrays and laser scanning cytometry. We demonstrated it can successfully capture and characterize rare tumor cells (several cells per mL) from mixed cell populations or even human whole blood, which fully justified the utility of this technology in clinical settings. This approach can also be applied to a variety of cytopathological examinations of rare cells, such as tumor stem cells from tissue biopsies and immune cell subtypes for informative immune monitoring. Using a high-content imaging cytometry approach, we show not only rapid counting of captured tumor cells but also quantitative analysis of functional parameters, such as cell shape and circularity at the single cell level. It has been reported that nanostructured substrates can alter cellular behavior, such as adhesion, spreading, and migration.[36−38] We performed capture of tumor cells on nanowire substrate and found size and morphology of A549 cells on QNW substrates were generally smaller and more rounded (less spreading) than the cells captured on smooth substrate (i.e., glass) (see Figure S10, Supporting Information), indicating that nanoscale topographic features do influence the cell capture and spreading. This is an interesting biological phenomenon, but it also means that we need to be cautious when we interpret the morphometric signatures of captured tumor cells in hope to identify CTC subtypes. In addition, it could be exploited to analyze other functional parameters, such as surface receptor expression and intracellular signaling proteins using immunocytochemistry, further enhancing the power of this integrated approach for distinguishing phenotypic diversity and functional heterogeneity of rare cells in hope of detecting the stem-like, metastasis-initiating circulating tumor cells from patients.

■ ASSOCIATED CONTENT

Supporting Information

Description of materials and experimental details including QNW fabrication, surface functionalization, cell preparation, and whole blood preparation. Description of additional results on flat glass and tumor cell capture from mixed cell population using imaging cytometry and quantitation of tumor cells from fresh blood samples. This material is available free of charge via the Internet at http://pubs.acs.org.

■ AUTHOR INFORMATION

Corresponding Author

*E-mail:sangkwon.lee@yale.edu; rong.fan@yale.edu.

Notes

The authors declare no competing financial interest.

■ ACKNOWLEDGMENTS

This study was supported by the U.S. National Cancer Institute Howard Temin Pathway to Independence Award (NIH 4R00 CA136759-02, PI: R.F.), the Priority Research Centers Program and by Basic Science Research Program through the National Research Foundation of Korea (NRF) funded by the Ministry of Education, Science and Technology (2010-0029706 and 2010-0019694, PI: S.-K.L.) and also partially supported by the Alzheimer's Association New Investigator Research Grant (PI: R.F.) and a grant from the KRIBB Research Initiative Program. S.-K.L. was supported by the Visiting Professor Program (2011) from the LG-Yonam foundation while visiting the Biomedical Engineering Department of Yale University. Y.W. is supported by the Anderson Postdoctoral Fellowship. S.-K.L. thanks Dr. H. Lim for initial quartz samples for the experiments and the fruitful discussion.

■ REFERENCES

(1) Yu, M.; Stott, S.; Toner, M.; Maheswaran, S.; Haber, D. A. *J. Cell Biol.* **2011**, *192*, 373−382.

(2) Pantel, K.; Brakenhoff, R. H.; Brandt, B. *Nat. Rev. Cancer* **2008**, *8*, 329−340.

(3) Chaffer, C. L.; Weinberg, R. A. *Science* **2011**, *331*, 1559−1564.
(4) Gupta, G. P.; Massagué, J. *Cell* **2006**, *127*, 679−695.
(5) Smerage, J. B.; Hayes, D. F. *Br. J. Cancer* **2006**, *94*, 8−12.
(6) Kim, S. I.; Jung, H.-i. *Int. J. Breast Cancer* **2010**, *13*, 125−131.
(7) Adeegbe, D.; Levy, R. B.; Malek, T. R. *Blood* **2010**, *115*, 1932−1940.
(8) Fujisaki, H.; Kakuda, H.; Shimasaki, N.; Imai, C.; Ma, J.; Lockey, T.; Eldridge, P.; Leung, W. H.; Campana, D. *Cancer Res.* **2009**, *69*, 4010−4017.
(9) Nagrath, S.; Sequist, L. V.; Maheswaran, S.; Bell, D. W.; Irimia, D.; Ulkus, L.; Smith, M. R.; Kwak, E. L.; Digumarthy, S.; Muzikansky, A.; Ryan, P.; Balis, U. J.; Tompkins, R. G.; Haber, D. A.; Toner, M. *Nature* **2007**, *450*, 1235−U10.
(10) Stott, S. L.; Lee, R. J.; Nagrath, S.; Yu, M.; Miyamoto, D. T.; Ulkus, L.; Inserra, E. J.; Ulman, M.; Springer, S.; Nakamura, Z.; Moore, A. L.; Tsukrov, D. I.; Kempner, M. E.; Dahl, D. M.; Wu, C.-L.; Iafrate, A. J.; Smith, M. R.; Tompkins, R. G.; Sequist, L. V.; Toner, M.; Haber, D. A.; Maheswaran, S. *Sci. Transl. Med.* **2010**, *2*, ra23.
(11) Fizazi, K.; Morat, L.; Chauveinc, L.; Prapotnich, D.; De Crevoisier, R.; Escudier, B.; Cathelineau, X.; Rozet, F.; Vallancien, G.; Sabatier, L.; Soria, J. C. *Ann. Oncol.* **2007**, *18*, 518−521.
(12) Danila, D. C.; Heller, G.; Gignac, G. A.; Gonzalez-Espinoza, R.; Anand, A.; Tanaka, E.; Lilja, H.; Schwartz, L.; Larson, S.; Fleisher, M.; Scher, H. I. *Clin. Cancer Res.* **2007**, *13*, 7053−7058.
(13) Cristofanilli, M.; Budd, G. T.; Ellis, M. J.; Stopeck, A.; Matera, J.; Miller, M. C.; Reuben, J. M.; Doyle, G. V.; Allard, W. J.; Terstappen, L.; Hayes, D. F. *N. Engl. J. Med.* **2004**, *351*, 781−791.
(14) Talasaz, A. H.; Powell, A. A.; Huber, D. E.; Berbee, J. G.; Roh, K.-H.; Yu, W.; Xiao, W.; Davis, M. M.; Pease, R. F.; Mindrinos, M. N.; Jeffrey, S. S.; Davis, R. W. *Proc. Natl. Acad. Sci. U.S.A.* **2009**, *106*, 3970−3975.
(15) Lee, J. Y.; Jones, C.; Zern, M. A.; Revzin, A. *Anal. Chem.* **2006**, *78*, 8305−8312.
(16) Kapur, R.; G. K. A.; Campana, M.; Adams, T.; Olson, K.; Jung, D.; Mrksich, M.; Vasudevan, C.; Taylor, D. L. *Biomed. Microdevices* **1999**, *2*, 11.
(17) Feigel, I. M.; Vedala, H.; Star, A. *J. Mater. Chem.* **2011**, *21*, 8940−8954.
(18) Jiang, X. Y.; Bruzewicz, D. A.; Wong, A. P.; Piel, M.; Whitesides, G. M. *Proc. Natl. Acad. Sci. U.S.A.* **2005**, *102*, 975−978.
(19) Shalek, A. K.; Robinson, J. T.; Karp, E. S.; Lee, J. S.; Ahn, D.-R.; Yoon, M.-H.; Sutton, A.; Jorgolli, M.; Gertner, R. S.; Gujral, T. S.; MacBeath, G.; Yang, E. G.; Park, H. *Proc. Natl. Acad. Sci. U.S.A.* **2010**, *107*, 1870−1875.
(20) Piret, G.; Galopin, E.; Coffinier, Y.; Boukherroub, R.; Legrand, D.; Slomianny, C. *Soft Matter* **2011**, *7*, 8642−8649.
(21) Kulangara, K.; Leong, K. W. *Soft Matter* **2009**, *5*, 4072−4076.
(22) Anselme, K.; Davidson, P.; Popa, A. M.; Giazzon, M.; Liley, M.; Ploux, L. *Acta Biomater.* **2011**, *7*, 1936−1937.
(23) Qi, S.; Yi, C.; Ji, S.; Fong, C.-C.; Yang, M. *ACS Appl. Mater. Interfaces* **2009**, *1*, 30−34.
(24) Lim, J. Y.; Hansen, J. C.; Siedlecki, C. A.; Runt, J.; Donahue, H. J. *J. R. Soc., Interface* **2005**, *2*, 97−108.
(25) Curtis, A. S. G.; Casey, B.; Gallagher, J. O.; Pasqui, D.; Wood, M. A.; Wilkinson, C. D. W. *Biophys. Chem.* **2001**, *94*, 275−283.
(26) Kwon, K. W.; Choi, S. S.; Lee, S. H.; Kim, B.; Lee, S. N.; Park, M. C.; Kim, P.; Hwang, S. Y.; Suh, K. Y. *Lab Chip* **2007**, *7*, 1461−1468.
(27) Kim, S. T.; Kim, D.-J.; Kim, T.-J.; Seo, D.-W.; Kim, T.-H.; Lee, S.-Y.; Kim, K.; Lee, K.-M.; Lee, S.-K. *Nano Lett.* **2010**, *10*, 2877−2883.
(28) Wang, S.; Wang, H.; Jiao, J.; Chen, K.-J.; Owens, G. E.; Kamei, K.-i.; Sun, J.; Sherman, D. J.; Behrenbruch, C. P.; Wu, H.; Tseng, H.-R. *Angew. Chem., Int. Ed.* **2009**, *48*, 8970−8973.
(29) Wang, S.; Liu, K.; Liu, J.; Yu, Z. T. F.; Xu, X.; Zhao, L.; Lee, T.; Lee, E. K.; Reiss, J.; Lee, Y.-K.; Chung, L. W. K.; Huang, J.; Rettig, M.; Seligson, D.; Duraiswamy, K. N.; Shen, C. K. F.; Tseng, H.-R. *Angew. Chem., Int. Ed.* **2011**, *50*, 3084−3088.
(30) Kim, J. S.; Cho, J. B.; Park, B. G.; Lee, W.; Lee, K. B.; Oh, M.-K. *Biosens. Bioelectron.* **2011**, *26*, 2085−2089.
(31) Lee, J.-H.; Kim, J. S.; Park, J.-S.; Lee, W.; Lee, K. E.; Han, S.-S.; Lee, K. B.; Lee, J. *Adv. Funct. Mater.* **2010**, *20*, 2004−2009.
(32) Shorte, S. *Cytometry, Part A* **2009**, *75A*, 711−711.
(33) Harnett, M. M. *Nat. Rev. Immunol.* **2007**, *7*, 897−904.
(34) Kim, S. T.; Kim, D. J.; Kim, T. J.; Seo, D. W.; Kim, T. H.; Lee, S. Y.; Kim, K.; Lee, K. M.; Lee, S. K. *Nano Lett.* **2010**, *10*, 2877−83.
(35) Institute, B.
(36) Kim, W.; Ng, J. K.; Kunitake, M. E.; Conklin, B. R.; Yang, P. D. *J. Am. Chem. Soc.* **2007**, *129*, 7228−+.
(37) Xie, C.; Hanson, L.; Xie, W. J.; Lin, Z. L.; Cui, B. X.; Cui, Y. *Nano Lett.* **2010**, *10*, 4020−4024.
(38) Shalek, A. K.; Robinson, J. T.; Karp, E. S.; Lee, J. S.; Ahn, D. R.; Yoon, M. H.; Sutton, A.; Jorgolli, M.; Gertner, R. S.; Gujral, T. S.; MacBeath, G.; Yang, E. G.; Park, H. *Proc. Natl. Acad. Sci. U.S.A.* **2010**, *107*, 1870−1875.